Published by :
http://www.ijert.org

International Journal of Engineering Research & Technology (IJERT)
ISSN: 2278-0181
Vol. 7 Issue 10, October-2018

Study on Three-Way Catalytic Converters and the use of Oxides as Reduction and Oxidation

Mayuranath Suresh Kumar
Department of Mechanical
Sri Ramakrishna Engineering College

Mohammed Haasheem. M
Department of Mechanical
Sri Ramakrishna Engineering College

Niyaz Ahmed. I
Department of Mechanical
Sri Ramakrishna Engineering College

***Abstract*-This is a study on catalytic converter to change the materials used in a conventional catalytic converter to replace noble metals and to introduce oxides as a catalyst, fusing oxides it is stated that emissions can be reduced. Since oxides act as both reduction and oxidation, conventional three-way catalytic converter can be reduced in steps to make a single way catalytic converter. Thus, this reduces size and cost**

1.INTRODUCTION

Automobiles predominantly use internal combustion petrol or diesel engines which burn hydrocarbons imperfectly and emit significant amounts of unburned HCs, CO and NO_x. These pollutants, in presence of sunlight and atmospheric water vapours react with each other to form secondary pollutants such as ozone, polyaromatic hydrocarbons (PAH), and photochemical smog, which is a mixture of complex organic substances, including peroxyacetyle nitrite (PAN). These emissions cause numerous health issues such as eye irritation, damage to breathing passage and lungs, reduces the oxygen carrying capacity of blood, causes premature death, increases infant mortality, and even causes damage at the ecosystem scale by causing acid rain.

In 2010, automotive emissions around the world caused about 180,000 deaths worldwide mainly by ischemic heart disease (91,000) and respiratory distress (34,000). Vehicular air pollution drew attention around the world in the 1950s and 1960s, as higher concentration of air pollution noticed in large cities like Los Angeles and Tokyo. As a remedy approach, catalytic converter was first introduced in USA in 1975 for curbing automotive emissions with great success. Subsequently, it was introduced in Japan, and later on Europe adopted the technology at industrial-scale in 1986. Catalytic converters reduce unburned hydrocarbons (HCs), carbon monoxide (CO) and nitrogen oxides (NO_x) into less toxic water vapor, carbon dioxide (CO_2), and nitrogen (N_2) to minimize negative impacts on health and environment. Regulatory agencies, particularly in USA, Japan, and Europe, enacted stringent emission standards for HCs, CO and NO_x around 1970 to control vehicular emissions.

In USA, catalytic converters significantly lowered the automobile originated HCs, NOx and CO emissions over the period 1970 to 1990. Global annual sales of catalytic converter also rose from just over 9 million units in 2006 to around 19 million units in 2012, and it will be around 140 million units by 2019. Evidently, catalytic converters are playing a significant role in saving human lives. On the other hand, catalytic converters pose substantial risks to lives as they contain platinum group metals (PGMs) which involves harmful mining and processing. In addition, risks on health and lives are also posed by the end-of-life recycling, and disposal of catalytic converters due to their PGM contents. Assessment of sustainability of a product, process or technology should encompass social, environmental, and economic wellbeing in order to avoid problem-shifting in the product system.

Life cycle assessment (LCA) is a sustainability assessment tool that considers both the reduction of emission by catalytic converters in their use and accounts for the negative impacts associated with the entire product life cycle of raw materials extraction to end-of-life disposal. According to a 2001 LCA study, catalytic converters reduce exhaust gas emissions during use phase, while they increase environmental burdens during production. Their study lacked in addressing the social impact in terms of human health of the catalytic converters throughout their life cycle. This journal deals with the numerous possibilities of variation of oxides which can be implemented in the catalytic converter.

2. EXPERIMENTAL PROCEDURE

2.1 Catalyst preparation

The monodispersed polymethyl methacrylate (PMMA) microspheres with the average diameter of 300 nm were prepared following a previously reported procedure. Three-dimensionally ordered macroporous (3DOM) $Ce_{0.8}M_{0.1}Zr_{0.1}O_2$ (M = Mn, Co, Ni) mixed oxide catalysts were synthesized by carboxy-modified colloidal crystal templating (CMCCT). The template synthesis was conducted at room temperature. $Ce(NO_3)_36H_2O$ (99.5%), $ZrOCl_28H_2O$ (98%), $Mn(NO_3)_2$ (49.0–51.0%), $Co(NO_3)_26H_2O$ (>98.5%) and Ni $(NO_3)_26H_2O$ (>98%) were used as the metal precursors. $Ce(NO_3)_36H_2O$, $ZrOCl_28H_2O$, and $M(NO_3)_xnH_2O$ (M = Mn, Co, Ni) were dissolved in the commixture of distilled water, ethylene glycol (EG) and methanol (EOH) (with the volume ratio of 10:7:3) under vigorous stirring for 40 min to obtain the precursor solution. After the stirring, a PMMA template was added into the precursor solution for 12 h to achieve full impregnation.

International Journal of Engineering Research & Technology (IJERT)
ISSN: 2278-0181
Vol. 7 Issue 10, October-2018

Subsequently, the solution was vacuum filtrated to remove the excess precursor solution and precipitate was dried at 50 C in the vacuum oven, followed by calcination in air for 10 h heating from room temperature to 550 C with the ramp rate of 1 C/min, thus generating 3DOM $Ce_{0.8}M_{0.1}Zr_{0.1}O_2$ (M = Mn, Co, Ni) mixed-oxide catalyst.

2.2 Catalyst characterisation

X-ray diffraction (XRD) was conducted with a powder X-ray diffractometer (Shimadzu XRD 6000) using Cu Ka radiation with a Nickel filter and the operating voltage and current of 40 kV and 10 mA, respectively. Nitrogen adsorption-desorption isotherms were performed at 196 C using an automatic TriStarII 3020 instrument. Scanning electron microscopic (SEM) images were obtained on a Quanta 200F instrument using accelerating voltages of 5 kV. The transmission electron microscope (TEM) images were obtained using a JEOl JEM 2100 electron microscope and 200 kV of accelerating voltage was used. Raman spectra of the samples were obtained in the anti-Stokes range of 100–2000 cm^1 using an in Via Reflex-Renishaw spectrometer. X-ray photoelectron spectra (XPS) were obtained using on a PerkinElmer PHI-1600 ESCA spectrometer with Mg Ka (hv = 1253.6 eV) as the X-ray source. Temperature programmed desorption of ammonia (NH_3-TPD) was performed using a Tianjin XQ TP-5076 conventional flow apparatus and was monitored by a thermal conductivity detector (TCD). Prior to the TPD measurements, each sample was degassed at 500 C for 1 h and then cooled down to 60 C and was then saturated with high purity anhydrous ammonia at 60 C for 1 h and flushed at the same temperature for 1 h in order to remove physiosorbed ammonium. Temperature-programmed reduction with H_2 (H_2-TPR) measurements were carried out on a chemical adsorption apparatus. Prior to H_2-TPR analysis, a 100 mg sample was pre-treated at 300 C in Ar for 1 h in order to remove the adsorbed water and carbon dioxide and was then cooled to room temperature. Then, 10% H_2/Ar flow (40 ml/min) was exposed to the catalyst bed and the hydrogen consumption signal was monitored on-line by a thermal conductivity detector (TCD).

In-situ diffuse reflectance infrared Fourier transform (DRIFT) spectra were recorded by a Thermo Nicolet Is50 spectrometer equipped with an MCT detector cooled by liquid nitrogen and a heating chamber. The catalyst was loaded in the Harrick IR cell and pretreated at 400 C under N_2 at the total flow rate of 100 ml/min for 60 min in order to remove the adsorbed impurities. A background spectrum was collected under a flowing through N_2 atmosphere and was subtracted from the sample spectrem. DRIFT spectra were recorded by accumulating 32 scans with the resolution of 4 cm^1.

2.3 Catalyst activity

The measurements of the simultaneous removal of PM and NO_x over 3DOM $Ce_{0.8}M_{0.1}Zr_{0.1}O_2$ (M = Mn, Co, Ni) catalysts were performed in a fixed bed quartz reactor (id = 10 mm). The composition of the feed gas was 1000 ppm NH_3, 1000 ppm NO, 3% O_2 and N_2 as the balance gas with the total flow of 100 ml/min. The performance of the optimum catalyst was also evaluated at a higher O_2 concentration (10%). Printex-U were used as model PM. Prior to each activity test, 100 mg catalyst and 10 mg PM were mixed with a spoon in order to obtain the loose contact that is similar to the circumstances of an actual diesel engine exhaust. The quartz wool was packed into the quartz tube to fix the mixture and avoid the axial diffusion. Each activity test was carried out from 30 to 600 C at the heating rate of 3 C/min. The concentration of the outlet gases, such as NH_3, NO, NO_2, N_2O, CO_2 and CO inclusive were monitored at the outlet of the catalyst by an online infrared spectrometer (Thermo Is50 FTIR) equipped with a 2.4 m gas cell. A fine and robust IR quantification method for multiple gaseous components were constructed (Qin and Cadet, 1997; Sinelli et al., 2010; Stec et al., 2011; Valencia et al., 2009). The standard gases with diverse intensity of different components were employed to draw the standard curves. The obtained standard curves were finally analysed by the TQ Analyst software. Precisions of the measurements have been guaranteed by successive refining the wavenumber ranges, correcting baselines, non-linear manners and components interactions. Prior to each measurement, the sample was swept by 100 ml/min N_2 approximately 45 min for the collection of the background spectrum. Then, the IR spectrum was recorded after purging with 1000 ppm NH_3, 1000 ppm NO, 3% O_2 and N_2 for 30 min in order to obtain a steady state. The data acquisition was performed at 3 C intervals from room temperature to 600 C. After the reaction, the capability of the catalyst for the oxidation of PM was represented by the PM combustion temperatures, and the temperature at the maximum combustion rate is denoted as T_m. The capability of the catalyst for NO_x reduction was evaluated by the maximal conversion of NO to N_2, and NO conversion was defined as

¼ ½NO^{inlet}½ ---------- ½NO^{outlet} 100%;

2.4 NO Conversion NO inlet.

The activate energy (Ea) of the catalytic reaction was measured. To fit the activation energy using the Arrhenius method, T_m was detected from room temperature to 873 K with the heating rates of 3, 5, 10 and 15 K/min. We can measure the change of the mass and temperature under non-isothermal condition, and estimate the value of the kinetic parameters from the plots displaying data of $\ln(a/T^2_m)$ versus 1/T to estimate the Ea for the reaction.

3. EXPERIMENTAL RESULTS

3.1 Catalytic activity

3.1.1 De-NOx performance of SCRPF catalysts

It is observed that the partial substitution of Ce with transition metal elements could indeed influence the SCR activity of the $Ce_{0.8}Zr_{0.2}O_2$ catalyst. Under identical operating conditions, among all 3DOM $Ce_{0.8}M_{0.1}Zr_{0.1}O_2$ (M = Mn, Co, Ni) catalysts, $Ce_{0.8}Mn_{0.1}Zr_{0.1}O_2$ sample exhibits the best performance with 100% NO conversion in the 374–512 C range. However, after the substitution by Co and Ni, 3DOM $Ce_{0.8}Co_{0.1}Zr_{0.1}O_2$ and 3DOM $Ce_{0.8}Ni_{0.1}Zr_{0.1}O_2$ catalysts seem to inhibit the NO conversion and show very narrow operation temperature windows. Both of the maximum NO conversion cannot reach 100%, obtaining

International Journal of Engineering Research & Technology (IJERT)
ISSN: 2278-0181
Vol. 7 Issue 10, October-2018

55% and 70%. These results suggest that different dopants give rise to various effects on the $Ce_{0.8}Zr_{0.2}O_2$ catalyst.
NH_3-SCR performance for the particle $Ce_{0.8}Zr_{0.2}O_2$ and $Ce_{0.8}Mn_{0.1}Zr_{0.1}O_2$ was also tested. Particle $Ce_{0.8}Zr_{0.2}O_2$ shows the maximal NO conversion of approximately 75% at 400 C, whereas 90% NO conversion was observed at 450 C for the particle Ce0.8Mn0.1Zr0.1O2.

3.1.2. PM oxidation over SCRPF catalysts

In practical applications, since the rate of PM oxidation at low temperatures is more important and cost-efficient for the entire purification process, we focus especially on the excellent catalytic activity at low T_m temperature. Table 1 lists T_m temperatures of PM and the temperature range of 100% NO conversion over 3DOM. $Ce_{0.8}M_{0.1}Zr_{0.1}O_2$ (M = Mn, Co, Ni) catalysts under loose contact condition. For the unsubstituted sample 3DOM $Ce_{0.8}Zr_{0.2}O_2$ in Table 1, T_m is 435 C for the catalytic combustion of PM; however, after the substitution by the transition metals, the catalytic activity values for these 3DOM $Ce_{0.8}M_{0.1}Zr_{0.1}O_2$ (M = Mn, Co, Ni) catalysts are different. In the case of 3DOM $Ce_{0.8}Mn_{0.1}Zr_{0.1}O_2$ catalysts, the Mn dopant remarkably enhances the catalytic activity for the removal of PM under loose contact conditions between the catalyst and PM, showing T_m value of 402 C. Whereas for 3DOM $Ce_{0.8}Co_{0.1}Zr_{0.1}O_2$ and $Ce_{0.8}Ni_{0.1}Zr_{0.1}O_2$ catalysts, the maximum catalytic PM combustion temperatures are approximately 433 and 429 C, respectively.

The particle $Ce_{0.8}Zr_{0.2}O_2$ and $Ce_{0.8}Mn_{0.1}Zr_{0.1}O_2$ exhibit remarkably high combustion temperature for PM oxidation. It is obvious that 3DOM $Ce_{0.8}Mn_{0.1}Zr_{0.1}O_2$ sample not only displays the lowest T_m temperature but also the widest NO conversion temperature range. Moreover, this temperature range is similar to the temperature of the exhaust pollutants emitted from the diesel engines. The catalytic activity for the simultaneous PM and NO_x abatement of the $Ce_{0.8}M_{0.1}Zr_{0.1}O_2$ (M = Mn, Co, Ni) samples are different due to the presence of different dopant. The $Ce_{0.8}Zr_{0.2}O_2$ catalyst required progressively higher temperatures to reach the maximal conversion for PM combustion and NO conversion (Shang et al., 2015).

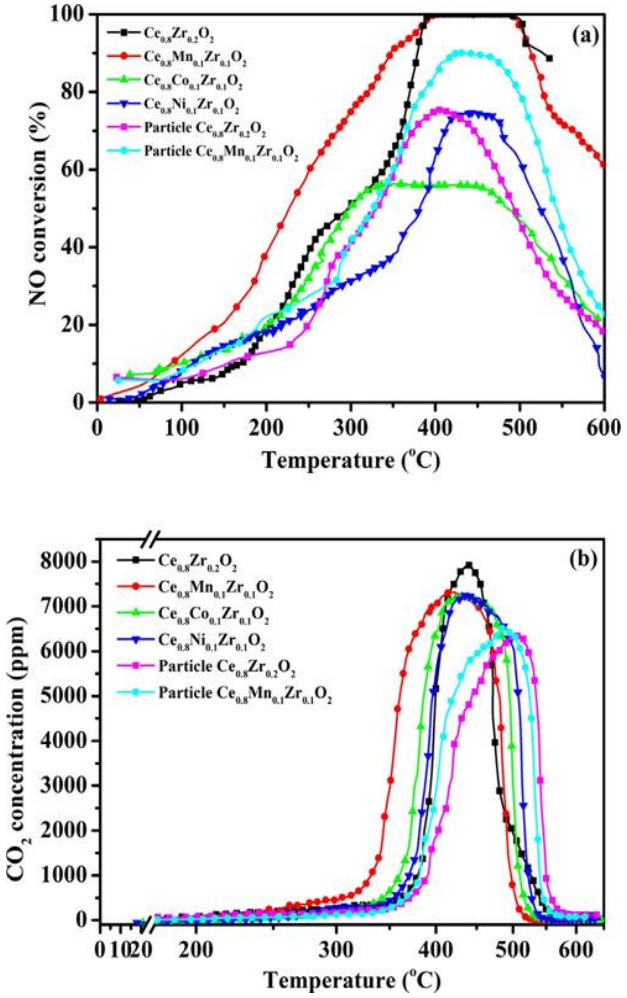

Figure 1: Temperature vs CO_2 and NO concentration

Figure 1 shows NO conversion and CO_2 concentration as a function of temperature for the simultaneous removal of PM and NOx over 3DOM $Ce_{0.8}M_{0.1}Zr_{0.1}O_2$ (M = Mn, Co, Ni) and particle catalysts in a gas feed containing 1000 ppm NH_3, 1000 ppm NO, 3% O_2 and balance N_2 at a gas hourly space velocity of 25,000 h^1.The experiment was performed for the simultaneous removal reaction under a high O_2 concentration (10%). Fig. S1 shows the catalytic activity over 3DOM $Ce_{0.8}Mn_{0.1}Zr_{0.1}O_2$ catalyst. The figure describes about the practical applications, since the rate of PM oxidation at low temperatures is more important and cost-efficient for the entire purification process, we focus especially on the excellent catalytic activity at low T_m temperature. Table 1 lists T_m temperatures of PM and the temperature range of 100% NO conversion over 3DOM. $Ce_{0.8}M_{0.1}Zr_{0.1}O_2$ (M = Mn, Co, Ni) catalysts under loose contact condition.
The following observation was observed for the above mentioned experimental procedures. The table shown below details the temperature for maximum concentration CO_2 (°C), the range of catalysts obtained and the achieved 100% NO conversion range.

International Journal of Engineering Research & Technology (IJERT)
ISSN: 2278-0181
Vol. 7 Issue 10, October-2018

Table 1: Effect induced by Various catalyst.

Catalyst	The temperature for maximum concentration CO_2 (°C)	CO_2 maximal concentration (ppm)	Achieved 100% NO conversion temperature range (C)
Ce0.8Zr0.2O2	435	7918	390–498
Ce0.8Mn0.1Zr0.1O2	402	7316	374–512
Ce0.8Co0.1Zr0.1O2	433	7244	55%
Ce0.8Ni0.1Zr0.1O2	429	7283	70%
Particle Ce0.8Zr0.2O2	507	6354	75%
Particle Ce0.8Mn0.1Zr0.1O2	486	6502	90%

From the Table it is clear that the increase of the O_2 concentration resulted in the decrease of the NH_3-SCR performance. 3DOM $Ce_{0.8}Mn_{0.1}Zr_{0.1}O_2$ catalyst showed rather high NO_x conversions of 100% within the 374–512 C operation temperature window under the 3% O_2 atmosphere. NO conversion above 80% could be found at 378–498 C under the 10% O_2 atmosphere, and the maximal NO conversion is 94%. Additionally, the maximum temperatures for PM combustion are 402 and 415 C, respectively. The promotion of the catalytic performance under high O_2 concentration should be addressed in future work.

3.2. Characterization of SCRPF catalysts

The patterns of 3DOM $Ce_{0.8}Zr_{0.2}O_2$ and various $Ce_{0.8}M_{0.1}Zr_{0.1}O_2$ (M = Mn, Co, Ni) samples are shown in Fig. S2 (in the supporting information). All main characteristic peaks are consistent with the face-centered cubic fluorite-like structure of CeO_2 (JCPDS PDF# 43-1002). 3DOM $Ce_{0.8}M_{0.1}Zr_{0.1}O_2$ (M = Mn, Co, Ni) catalysts exhibit typical diffraction peaks belonging to CeO_2, indicating that the dopant does not change the cubic structure of the catalysts. These lattice planes assigned to (111), (200), (220), (311), (222), (400), (331), (420) and (422) could be detected.

Fig. S3 shows the type II characteristic isotherm accompanied with H3 hysteresis loop in the relative high pressure (P/P_0) range and a nearly linear correlation in the low-pressure range.

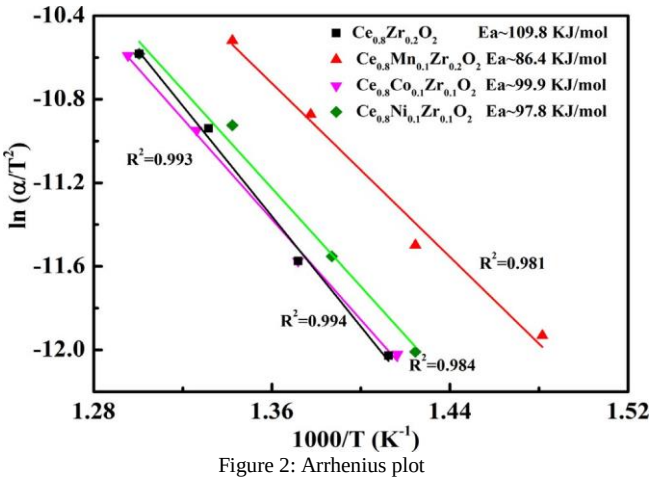

Figure 2: Arrhenius plot

Figure 2. Arrhenius plot of simultaneous removal of PM and NO conversion over exposure of 3DOM $Ce_{0.8}M_{0.1}Zr_{0.1}O_2$ (M = Mn, Co, Ni) catalysts loosely mixed with PM with a different rate of 3 K/min, 5 K/min, 10 K/min, 15 K/min. (gas feed contains 1000 ppm NH_3, 1000 ppm NO, 3% O_2 and balance N_2 at a gas hourly space velocity of 25,000 h^1).

The finding is observed due to the unrestricted monolayer-multilayer adsorption,whereas the appearance of the H3 hysteresis loop is an indication of the macroporous structure (Li et al., 2013; Wang et al., 2013). In the case of 3DOM Ce0.8Co0.1Zr0.1O2 and Ce0.8Ni0.1Zr0.1O2 catalysts, there are weak adsorption peaks at approximately 220 and 670 cm^1 that could be assigned to the CoAO and NiAO stretching vibrations in the samples. This suggested that Co and Ni species should be present on the $Ce_{0.8}Zr_{0.2}O_2$ surface. On the other hand, no Raman lines due to MnAO are observed for $Ce_{0.8}Mn_{0.1}Zr_{0.1}O_2$. Therefore, Mn is probably inserted into the $Ce_{0.8}Zr_{0.2}O_2$ lattice to form solid solutions as shown in Fig. S4.

XPS is a powerful technique for the exploration of the electronic properties of surface element components, metal oxides states and adsorbed oxygen species of the catalysts. Fig. 4 depicts Ce 3d, O 1s XPS spectra of 3DOM $Ce_{0.8}M_{0.1}Zr_{0.1}O_2$ (M = Mn, Co, Ni) catalysts, and the corresponding quantitative analytic results are summarized in Table 2. It can be observed that the Ce3d spectra are split into eight peaks labeled V (881.9 eV), V0 (884.1 eV), V00(888.6 eV), V^{000} (897.8 eV), U (900.4 eV), U0 (902.7 eV), U00 (907.2 eV), U^{000} (916.3 eV). The decomposed peaks centered at V, V00, V^{000}, U, U00, U^{000} are attributed to the $3d^{10}4f^0$ state of Ce^{4+} species, and the peaks assigned to V0 and U0 correspond to the $3d^{10}4f^1$ state of Ce^{3+} species (Trovarelli, 1999). In Table 2, we observe a minor discrepancy in the surface Ce^{3+}/Ce^{4+} ratio of these 3DOM $Ce_{0.8}M_{0.1}Zr_{0.1}O_2$.

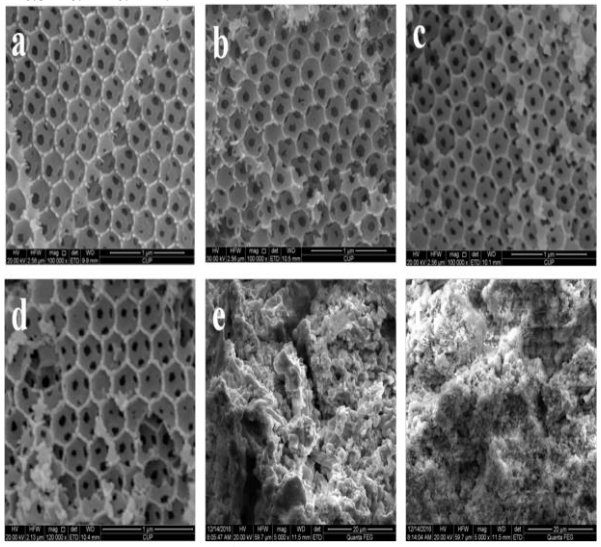

Figure 3: Images of Honey comb structure under SEM

Figure. 3. SEM images of 3DOM catalysts (a) Ce0.8Zr0.2O2 (b) Ce0.8Mn0.1Zr0.1O2 (c) Ce0.8Co0.1Zr0.1O2 (d) Ce0.8Ni0.1Zr0.1O2 (e) particle Ce0.8Zr0.2O2 (f) particle Ce0.8Mn0.1Zr0.1O2. It shows

International Journal of Engineering Research & Technology (IJERT)
ISSN: 2278-0181
Vol. 7 Issue 10, October-2018

the representative SEM images of 3DOM $Ce_{0.8}M_{0.1}Zr_{0.1}O_2$ (M = Mn, Co, Ni) and particle samples. It is observed that after calcination at 550 C, all samples (a–d) display a high quality 3DOM structure possessing a skeleton surrounding a uniform periodic arrangement of voids with the average diameter of 300 ± 20 nm and the wall thickness of 25 nm, which is smaller than the 400 nm of the PMMA spheres. For 3DOM samples, all catalysts have the uniform pore size, windows and wall thickness, and these macrospores are highly periodically arrayed and interconnected with the small windows. Obviously, the next layer is also visible in SEM image and is strongly interconnected through the opening windows. According to SEM result shown in Figure. 3, it is clear that 3DOM $Ce_{0.8}M_{0.1}Zr_{0.1}O_2$ (M = Mn, Co, Ni) catalysts show the similar 3DOM architecture with 3DOM $Ce_{0.8}Zr_{0.2}O_2$, indicating that the dopant does not induce significant changes in 3DOM architecture. However, the particle samples show the irregular structure.

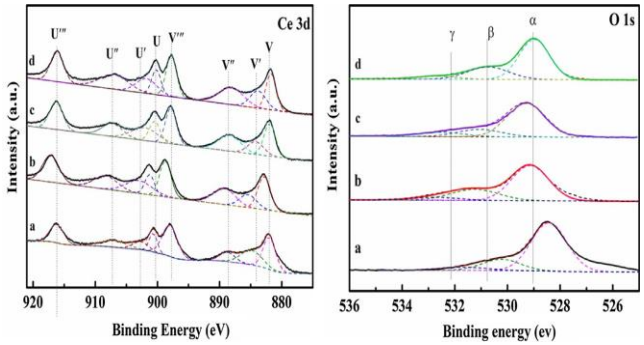

Figure 4: XPS result linking binding energy and intensity

Table 2: Surface composition and oxidation state of Ce 3d and O1s over 3DOM catalyst by XPS analysis.

Samples	Ce^{3+} (%)	Ce^{4+} (%)	Rb	O (%)	O_2 (%)	O^2 (%)	Rc
Ce0.8Zr0.2O2	22.5	77.5	0.290	7.5	19.8	72.7	0.376
Ce0.8Mn0.1Zr0.1O2	24.8	75.2	0.33	6.2	24.4	69.4	0.441
Ce0.8Co0.1Zr0.1O2	23.6	76.4	0.309	6.1	23.2	70.8	0.412
Ce0.8Ni0.1Zr0.1O2	22.3	77.7	0.287	6.2	20.7	71.8	0.375

It can be deduced that the interaction between cerium and the dopant may lead to transfer of the lattice oxygen in the ceria over the surface, maintaining the low-valent state of cerium. Among 3DOM $Ce_{0.8}M_{0.1}Zr_{0.1}O_2$ (M = Mn, Co, Ni) samples, 3DOM $Ce_{0.8}Mn_{0.1}Zr_{0.1}O_2$ sample exhibits the highest surface Ce^{3+}/Ce^{4+} ratio (the value of R^b). The increase of the Ce^{3+} content is due to the interaction between cerium and the surrounding atoms that leads to an increase in the oxygen vacancies. However, after the substitution by Co and Ni, it leads to a drop of the surface Ce^{3+}/Ce^{4+} ratio. This evidence is mainly due to the formation of CoO_x and NiO_x on the surface of 3DOM Ce0.8Co0.1Zr0.1O2 and 3DOM Ce0.8Ni0.1Zr0.1O2 samples, further implying that the interaction between the dopant and CeO_2 varies. Concurrently, it is reported that a rise in Ce^{3+} favors the increase in the number of the oxygen vacancies and the relatively high mobility of the bulk oxygen species (Du et al., 2012; Krishna et al., 2007; Wei et al., 2012).

$Ce_{0.8}M_{0.1}Zr_{0.1}O_2$ catalysts. According to the curve fitting methods, O1s can be decomposed to three dominant peaks a(529.1 eV), b (530.7 eV), c(532.2 eV), which ascribes to the lattice oxygen (O^2) and chemical adsorbed oxygen (O, O_2), respectively. As is known, the adsorbed oxygen is viewed as the dominant active oxygen species and plays a dominant role in the redox reaction. In other words, the O_{ads}/O_{latt} ratio could reflect the content of active oxygen species of the reaction. Table 2 shows that 3DOM $Ce_{0.8}$-$Mn_{0.1}Zr_{0.1}O_2$ sample possesses the highest O_{ads}/O_{latt} ratio and Ce^{3+} concentration. A Ce-based catalyst with abundant oxygen vacancies and defects is an effective catalyst. The reduction of Ce^{4+} to Ce^{3+} in ceria facilitates the formation of oxygen vacancies, further promoting the oxygen escaping from the lattice sites and leaving vacant sites with two electrons at each vacancy. (Arandiyan et al., 2015) Furthermore, the abundant active oxygen is beneficial for the oxidation of PM.

H_2-TPR analysis is an ideal tool for measuring the reduction behaviour of the catalysts. The reducibility of the metallic ion from high to low valence, and the nature of taking up oxygen as well as the species of the absorbed oxygen or activated could be reflected in this analysis. H_2-TPR profiles of 3DOM $Ce_{0.8}M_{0.1}Zr_{0.1}O_2$ (M = Mn, Co, Ni) catalysts are shown in Fig. 5. It can be observed that distinct reduction peaks centered at 565 C are found for 3DOM $Ce_{0.8}Zr_{0.2}O_2$ sample. The low temperature reduction peak is probably due to the reduction of Ce^{4+} to Ce^{3+} ions in the outermost layers as well as the reduction of the surface capping oxygen of CeO_2. Interestingly, after the introduction of metal and Zr ions into CeO_2, the reduction peaks shift to the low temperature range, indicating that the mobility of surface lattice oxygen species is generally improved by the dopant. The improvement is mainly the result of the synergistic effect between the dopants and CeO_2. For 3DOM $Ce_{0.8}Mn_{0.1}Zr_{0.1}O_2$ sample, the initial reduction peak centered at 486 C is due to the reduction of surface adsorption oxygen species, while the high reduction peak is the result of the reduction of lattice oxygen and the inner Ce^{4+}

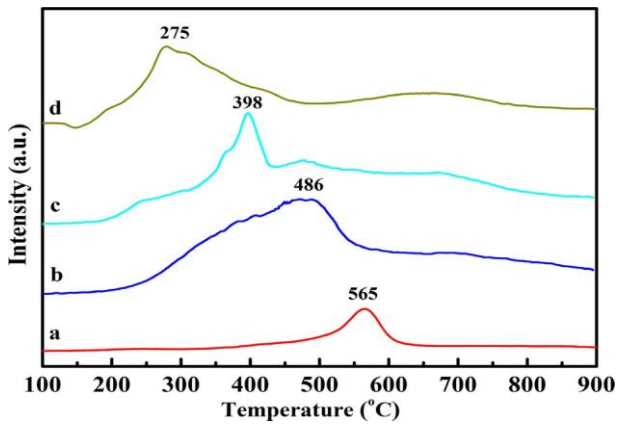

Figure 5: H_2-TPR of 3DOM catalysts

International Journal of Engineering Research & Technology (IJERT)
ISSN: 2278-0181
Vol. 7 Issue 10, October-2018

The obvious reduction attributing to Mn could be detected, further confirming the formation of a CeAMnAZrAO solid solution (Töpfer and Goodenough, 1997). However, relatively low temperature reduction peaks appear in 3DOM $Ce_{0.8}Co_{0.1}Zr_{0.1}O_2$ and 3DOM $Ce_{0.8}Ni_{0.1}Zr_{0.1}O_2$ catalysts, which is in accordance with the reduction of CoO_x and NiO_x. Considering the results of Raman and TEM analyses, the appearance of low temperature reduction peaks may be ascribed to the reduction of CoO_x and NiO_x, respectively. This phenomenon indicates that CoO_x and NiO_x are present on the surface of the catalyst. It is generally accepted that the formation of a CeO_2-based solid solution could improve the reducibility of the materials. Using Mn doped into the CeAZr mixed oxidation, CeAMnAZrAO solid solutions can be easily obtained. Nevertheless, the doping of Co and Ni may cause strong sintering of the CoO_x and NiO_x nanoparticles, which would result in the shift of the reduction peaks to low temperatures (Li et al., 2013; Shang et al., 2015; Zhou et al., 2016). It is noted that among these catalysts, 3DOM $Ce_{0.8}Mn_{0.1}Zr_{0.1}O_2$ catalyst display better reacting behaviors toward H_2 consumption at the lower temperatures. Evidently, the introduction of Mn with molar concentration of 0.1 promotes the reducibility of the catalysts.

It can be speculated that the formation of a more homogeneous of CeAMnAZrAO tenerary solid solution may give better catalytic performances for the simultaneous removal of PM and NO_x from diesel engine exhausts. $Ce_{0.8}Zr_{0.2}O_2$ and $Ce_{0.8}M_{0.1}Zr_{0.1}O_2$ (M = Mn, Co, Ni) catalysts with the results shown in Fig. 6. Interestingly, it is obvious that each catalyst shows a strong peak centered below 200 C, characteristic of the weakly physical desorption of NH_3 or the ammonium species adsorbed at weak acid sites (Cheng et al., 2015; Martins et al., 2008; Onida et al., 1996). The peak in 250– 450 C is due to the ammonia adsorbed at mid-strong acid sites. The peak above 470 C may belong to strong acid sites arising from the interaction between CeO_2 and the doped element. Analyzing the amounts of NH_3 desorption, we conclude that the introduction of a dopant plays a positive role for providing the acid sites. NH_3TPD peak of 3DOM $Ce_{0.8}Zr_{0.2}O_2$ is much lower than those of 3DOM $Ce_{0.8}M_{0.1}Zr_{0.1}O_2$ (M = Mn, Co, Ni) samples. In addition, it is generally accepted that the peak location is closely related to the adsorption strength and the peak area corresponds well to the amount of adsorbed NH_3. Therefore, the modification of $Ce_{0.8}Zr_{0.2}O_2$ by transition metals could enhance the surface acidity of $Ce_{0.8}Zr_{0.2}O_2$. Moreover, the stronger acidity of 3DOM $Ce_{0.8}M_{0.1}Zr_{0.1}O_2$ increases its NH_3 adsorption capacity. This is favorable to NH_3-SCR reaction. Doping with Mn promotes the formation of active acid sites and is beneficial for the adsorption and activation of NH_3.

In-situ DRIFT experiments were also employed to explore the NH3 desorption behavior on the catalysts. In-situ DRIFT of NH_3 adsorption was conducted to examine the change of acidity on the catalyst with the results presented in Fig. 7. The bands at 1159 and 1313 cm^1 are related to the coordinated NH_3 bound to Lewis acid sites. The band at approximately 1341 cm^1 is characteristic for the ANH_2 species. The band at 1443 cm^1 is attributed to the NH^{4+} species on the Brønsted acid, which is due to the asymmetric bending vibration of the NAH bond in the ANH^{3+} group, generated from the decomposition of the NH^{4+} chemisorbed on a Brønsted acid site. For 3DOM $Ce_{0.8}Zr_{0.2}O_2$ catalysts, only the bands at 1159, 1313 and 1341 cm^1 could be detected, which are due to the NH_3 adsorption on the Lewis acid sites and ANH_2 species, respectively. For 3DOM $Ce_{0.8}Mn_{0.1}Zr_{0.1}O_2$ catalysts, obvious bands at 1065, 1159, 1313, 1341, 1443 and 1539 could be detected, characteristic for the Lewis acid sites, Brønsted acid as well as ANH^{3+} group and ANH_2 species. Compared with 3DOM $Ce_{0.8}Co_{0.1}Zr_{0.1}O_2$ and $Ce_{0.8}Ni_{0.1}Zr_{0.1}O_2$ samples, the bands at 1159 and 1341 cm^1 ascribed to Lewis acid sites and ANH_2 species can be detected. This differences show that the dopants of different transition metal into $Ce_{0.8}Zr_{0.2}O_2$ deeply affect the NH_3 adsorption and activation. More acid sites could be detected on the Mn-doped samples. The adsorption and activation of NH_3 promotes the formation of active acid sites. After the Mn dopant, Ce-Zr mixed oxides is prone to produce more ANH^{3+} group that can easily combine with NO to produce NO_3 , which is beneficial for PM combustion.

In-situ DRIFT spectra over 3DOM catalysts at 400 C in a flow of 1000 ppm NH_3+ 1000 ppm NO+ 3% O_2. For 3DOM $Ce_{0.8}M_{0.1}Zr_{0.1}O_2$ (M = Mn, Co, Ni) samples, several bands at 1159, 1341, 1443, 1536 cm^1 could be observed. The band at 1159 cm^1 is related to the coordinated NH_3 bound to Lewis acid sites, and the bands at 1443 cm^1 is attributed to the NH^{4+} species on Brønsted acid. The band at 1536 cm^1 is attributed to the asymmetric bending vibration of the NAH bond in the ANH^{3+} group, generated from the decomposition of NH^{4+} chemisorbed on Brønsted acid site. The bands at 1341 cm^1 are related to the scissoring and wagging vibrations of the ANH_2 species formed by hydrogen abstraction from the NH_3 coordinated to Lewis acid sites. Whereas for 3DOM $Ce_{0.8}Zr_{0.2}O_2$ samples, only bands at 1159, 1341, 1445 cm^1 could be observed. For 3DOM $Ce_{0.8}Mn_{0.1}Zr_{0.1}O_2$ catalysts, obvious bands at 1159, 1289, 1341, 1443 and 1536 cm^1 could be detected, characteristic for monodentate nitrate, bidentate nitrate, respectively.

Only band at 1289 and 1443 cm^1 were observed for 3DOM $Ce_{0.8}Co_{0.1}Zr_{0.1}O_2$ and 1159, 1289 and 1443 cm^1 for 3DOM $Ce_{0.8}Ni_{0.1}Zr_{0.1}O_2$ samples. It is evident that there are many bands ascribed to NH^{4+} and ANH_2 species on 3DOM $Ce_{0.8}M_{0.1}Zr_{0.1}O_2$ catalysts, promoting PM oxidation and NO reduction.

4. EXPERIMENTAL VALIDATION

4.1. Influence of the structure on the performance of 3DOM

The reaction of PM combustion is a typical heterogeneous catalysis reaction that occurs at the three-phase boundary among a solid catalyst, a solid reactant (PM), and gaseous reactants (O_2, NO). Thus, a vital issue strongly influencing the catalytic activity of a catalyst for the solid-solid reaction is the contact conditions between PM and the catalyst. As revealed by many studies, the catalytic performance of catalysts for PM combustion is very excellent under tight condition between PM and the catalyst due to their good contact condition. However, this cannot meet the practical contact condition because catalysts on the

International Journal of Engineering Research & Technology (IJERT)
ISSN: 2278-0181
Vol. 7 Issue 10, October-2018

surface of the filter and PM are in loose contact (Oi-Uchisawa et al., 2003), weakening the catalytic effect between catalysts and PM. Thus, it is significantly necessary to study and design the active catalysts for PM combustion under loose contact conditions. Even though numerous nanoparticle catalysts show remarkable catalytic activities for PM combustion (Liu et al., 2009), the catalytic activities of these catalysts are still decreased considering that their small pore sizes limit the transport of PM into their inner pore, making less full use of the inner active site. Thus, the efficiency of a catalyst is strongly influenced by the contact between PM and the catalyst. The contact between catalyst active sites and PM must be improved for process intensification. In this work, 3DOM catalysts possess special large pore size and ordered interconnected macrosporous tunnels structure, and the window size is approximately 300 nm, which are much larger than the size of PM (approximately 25 nm, Fig. S6). Moreover, this special structure can permit PM to diffuse easily into the inner 3DOM catalysts by the airflow in the reaction and shows less resistance for transport through the catalyst structure. The catalyst is in close proximity with PM and more catalyst surface is exposed to reaction atmosphere. As shown in

4.2. Influence of NH_3 and different dopant

Even though there are many reports on the simultaneous abatement of PM and NO_x from diesel engines (Milt et al., 2008; Wang et al., 2014), few investigation have been performed regarding the concentration of the reducing gas and almost no reducing gas was used. Thus, these catalysts exhibited low NO conversion. In general, it is challenging to reduce NO_x under the oxygen-rich conditions. To improve the efficiency of NO conversion, different dopants are also added into the CeAZr mixed oxides. Based on NH_3-TPD analysis, $Ce_{0.8}M_{0.1}Zr_{0.1}O_2$ shows a high acid amount and acid strength than those of the $Ce_{0.8}Zr_{0.2}O_2$ sample, indicating that the dopant is beneficial for increasing the acid amount and strength of 3DOM $Ce_{0.8}Zr_{0.2}O_2$. The bands at 1539 and 1341 cm^1 are also observed. The latter is related to scissoring and wagging vibrations of the ANH_2 species, formed by hydrogen abstraction from NH_3 coordinated to a Lewis acid site. For the $Ce_{0.8}Mn_{0.1}Zr_{0.1}O_2$ catalyst, the bands at 1065, 1159, 1341, 1443 and 1539 cm^1 could be obviously observed, while for 3DOM $Ce_{0.8}Co_{0.1}Zr_{0.1}O_2$ and $Ce_{0.8}Ni_{0.1}Zr_{0.1}O_2$ catalyst, the band at 1443 cm^1 attributed to the NH^{4+} species on Brønsted acid is absent. NH^{3+} as an intermediate product is prone to react with NO to produce N_2, which is beneficial for the conversion of NO to N_2 and promotes the NH_3-SCR reaction. This indicates that more NH_3 will be adsorbed and activated over $Ce_{0.8}M_{0.1}Zr_{0.1}O_2$ (M = Mn, Co, Ni) catalyst. The addition of Mn can enhance NH_3 adsorption and activation. Moreover, the active acid sites easily absorb NH_3 molecules and produce more NH^{4+} species, which is also beneficial for the improvement of the catalytic activity for NO reduction.

5. CONCLUSION

The new SCRPF combining catalyst technology is an efficient and economical approach for purification of PM and NOx from diesel engine exhaust. For the simultaneous removal of PM and NO, a series of highly ordered monolithic 3DOM $Ce_{0.8}M_{0.1}Zr_{0.1}O_2$ (M = Mn, Co, Ni) catalysts are successfully prepared by a colloidal crystal template method. The diffusion and combustion reaction of PM and the reduction of NO_x are process intensified by the unique 3DOM structure and the doping metal ions. Thus the following conclusions were made from the various references involved. 3DOM $Ce_{0.8}M_{0.1}Zr_{0.1}O_2$ (M = Mn, Co, Ni) sample possesses high-quality 3DOM architecture exhibiting better low temperature reducibility than 3DOM $Ce_{0.8}Zr_{0.2}O_2$.

The Ce^{3+}/Ce^{4+} ratio and the surface-active oxygen species on 3DOM $Ce_{0.8}Mn_{0.1}Zr_{0.1}O_2$ are much higher than those on the other 3DOM $Ce_{0.8}M_{0.1}Zr_{0.1}O_2$ (M = Mn, Co, Ni) catalysts. 3DOM $Ce_{0.8}Mn_{0.1}Zr_{0.1}O_2$ sample presented the most pronounced catalytic activity with the maximum concentration of CO_2 at 402 C and nearly a 100% NO conversion in the 374–512 C range, achieving the purposes of the removal of PM and NOx within the same temperature range. 3DOM $Ce_{0.8}Mn_{0.1}Zr_{0.1}O_2$ exhibits the lowest Ea value (86.4 kJ/mol), while the lower active energy remarkably reduces the reaction energy barrier. This is more conductive for the catalytic reaction to proceed smoothly.

Hence, various oxides can be used to follow out the oxidation and reduction process as the suitable catalyst chemicals. Of these oxide, depending on the cost, time taken for conversion of harmful gases to less harmful ones and affecting temperature, the required oxides can be selected and used. Thus this journal deals with the numerous possibilities of variation of oxides which can be implemented in the catalytic converter.

6. REFERENCES

[1] Arandiyan, H., Dai, H., Ji, K., Sun, H., Zhao, Y., Li, J., 2015. Enhanced catalytic efficiency of Pt nanoparticles supported on 3D ordered macro-/mesoporous $Ce_{0.6}$ $Zr_{0.3}$ $Y_{0.1}O_2$ for methane combustion. Small 11, 2366–2371.

[2] Atribak, I., Buenolopez, A., Garciagarcia, A., 2008. Combined removal of diesel soot particulates and NOx over CeO_2–ZrO_2 mixed oxides. J. Catal. 259, 123–132.

[3] Cheng, K., Liu, J., Zhao, Z., Wei, Y., Jiang, G., Duan, A., 2015. Direct synthesis of V-W– Ti nanoparticle catalysts for selective catalytic reduction of NO with NH_3. RSC Adv. 5, 45172–45183.

[4] Choi, B., Lee, K.-S., 2014. LNT/CDPF catalysts for simultaneous removal of NO_x and PM from diesel vehicle exhaust. Chem. Eng. J. 240, 476–486.

[5] Di Sarli, V., Di Benedetto, A., 2015. Modeling and simulation of soot combustion dynamics in a catalytic diesel particulate filter. Chem. Eng. Sci. 137, 69–78.

[6] Diehl, F., Barbier, J., Duprez, D., Guibard, I., Mabilon, G., 2015. Catalytic oxidation of heavy hydrocarbons over Pt/Al_2O_3. Oxidation of C^{10+} solid hydrocarbons representative of soluble organic fraction of Diesel soots. Appl. Catal. A: Gen. 504, 37–43.

[7] Du, X., Zhang, D., Shi, L., Gao, R., Zhang, J., 2012. Morphology dependence of catalytic properties of Ni/CeO_2 nanostructures for carbon dioxide reforming of methane. J. Phys. Chem. C 116, 10009–10016.

[8] Martins, G., Berlier, G., Bisio, C., Coluccia, S., Pastore, H., Marchese, L., 2008. Quantification of Brønsted acid sites in microporous catalysts by a combined FTIR and NH_3-TPD study. J. Phys. Chem. C 112, 7193–7200.

[9] Metkar, P.S., Harold, M.P., Balakotaiah, V., 2013. Experimental and kinetic modeling study of NH_3-SCR of NOx on Fe-ZSM-5, Cu-chabazite and combined Fe- and Cuzeolite monolithic catalysts. Chem. Eng. Sci. 87, 51–66.

International Journal of Engineering Research & Technology (IJERT)
ISSN: 2278-0181
Vol. 7 Issue 10, October-2018

[10] Milt, V.G., Banús, E.D., Ulla, M.A., Miró, E.E., 2008. Soot combustion and NOx adsorption on Co, Ba, K/ZrO_2. Catal. Today 133–135, 435–440.
[11] Oi-Uchisawa, J., Obuchi, A., Wang, S., Nanba, T., Ohi, A., 2003. Catalytic performance of Pt/MOx loaded over SiC-DPF for soot oxidation. Appl. Catal. B 43, 117–129.
[12] Onida, B., Gabelica, Z., Lourenco, J., Garrone, E., 1996. Spectroscopic characterization of hydroxyl groups in SAPO-40. 1. Study of the template-free samples and their interaction with ammonia. J. Phys. Chem. 100, 11072–11079.
[13] Raj, A., Zainuddin, Z., Sander, M., Kraft, M., 2011. A mechanistic study on the simultaneous elimination of soot and nitric oxide from engine exhaust. Carbon 49, 1516–1531
[14] Shangguan, W., Teraoka, Y., Kagawa, S., 1997. Kinetics of soot-O_2, soot-NO and sootO_2-NO reactions over spinel-type $CuFe_2O_4$ catalyst. Appl. Catal. B 12, 237–247